Inclusions embedded in lipid membranes

2001 J. Phys. A: Math. Gen. 34 439

(http://iopscience.iop.org/0305-4470/34/3/309)

INSTITUTE OF PHYSICS PUBLISHING JOURNAL OF PHYSICS A: MATHEMATICAL AND GENERAL

J. Phys. A: Math. Gen. **34** (2001) 439–459 www.iop.org/Journals/ja PII: S0305-4470(01)13890-4

Inclusions embedded in lipid membranes

Paolo Biscari[1,3] **and Riccardo Rosso**[2,3]

[1] Dipartimento di Matematica, Politecnico di Milano, Piazza Leonardo da Vinci 32, 20133 Milano, Italy
[2] Dipartimento di Matematica, Università di Pavia, Via Ferrata 1, 27100 Pavia, Italy
[3] Istituto Nazionale di Fisica della Materia, Via Ferrata 1, 27100 Pavia, Italy

Received 10 May 2000, in final form 14 September 2000

Abstract

We study the equilibrium of lipid membranes embedding a protein, conceived as a rigid inclusion. By use of a two-dimensional model, we are able to determine the exact equilibrium shape of the membrane, which is idealized as a closed curve. We also discuss the role played by the anchoring of the protein to the membrane. When the anchoring is strong, we are always able to find different classes of equilibrium shapes and, within them, to assess the uniqueness of regular equilibrium configurations. In contrast, the presence of a weak anchoring yields a loss of uniqueness within each class, and even a loss of any regular equilibrium configuration, if the spontaneous curvature exceeds a critical value, which increases with the anchoring strength. In this case, suitable singular solutions are found, where the protein is segregated from the rest of the membrane. These solutions mimic the behaviour of coat proteins in lipid membranes, suggesting that weak anchoring could be invoked as a possible mechanism to induce protein segregation. A resort to numerical techniques provides us with a comprehensive view of the problem.

PACS number: 4670H

AMS classification scheme numbers: 73C50, 76Z99

1. Introduction

Great efforts have been devoted in the last two decades to investigate the behaviour of proteins embedded in lipid membranes, mainly because it has been recognized that many biologically important properties of lipid membranes are due to the presence of proteins within them. Lipid membranes are aggregates of *amphipathic* molecules, which consist of a *hydrophilic* head and one or two *hydrophobic* tails. In an aqueous environment, these molecules tend to form *bilayers* where the hydrophobic parts are hidden by the hydrophilic ones, and so their contact with water is reduced. A further reduction is obtained when the bilayer closes itself to form a *vesicle*, which is modelled as a compact, two-dimensional surface. A peculiarity of vesicles is that their molecules are not likely to leave the membrane. This feature can be

embodied in a mathematical treatment, by prescribing the area of the vesicle. A constraint on the volume enclosed by the vesicle has been often imposed too, even if it is possible to relax it when the osmotic pressure is negligible (see, for instance, Dommersnes *et al* [5]), that is, when 'the aqueous fluid environment is essentially free of molecules that cannot permeate the bilayer membrane', as remarked by Jülicher and Lipowsky [11].

Proteins, thought of as rigid bodies, are usually modelled as either cylinders or cones. Once embedded in a lipid membrane, they modify the membrane configuration in two ways: first, they have a *hydrophobic* belt whose height may be different from the thickness of the membrane, giving rise to a *hydrophobic mismatch*. The large energetic cost of an exposure of the hydrophobic belt to water causes a deformation of the membrane in the region surrounding the protein. Three different deformation modes have been studied in the literature, by exploiting the analogy existing between a lipid bilayer and a smectic-A liquid crystal (Helfrich and Jakobsson [9]): a *compression–expansion* mode, related to changes in the bilayer thickness nearby the protein, a *splay* mode, due to a tilt of the amphipathic molecules with respect to the layer's normal, and a *surface-tension* mode, related to changes in the density of the polar head groups. As a result, this latter term is always negligible in the case of thin bilayers, which confirms that, in this situation, surface tension is irrelevant (see, e.g., Jähnig [10]). Proteins also affect the equilibrium shape of the membrane within which they exist, a feature that has been underlined on studying long-range interactions between embedded proteins [8]. In this case, the membrane and the proteins are usually thought of as being orthogonal to each other at their interface, whereas thickness variations are neglected. Essentially, looking at either deformations in membrane thickness or shape deformations amounts to adopting two different length scales.

The choice of the appropriate boundary conditions at the protein–membrane interface is a rather delicate matter, which also depends on the length scale used to look at the protein. If attention is focused on the hydrophobic matching, and so on a length scale where thickness deformations induced by the proteins are relevant, it is possible to account for interactions between the membrane and the proteins by fixing the *contact angle* between them, that is, the angle formed by the layers' and the protein's normals at the interface (see, e.g., [1]). A somewhat different approach was introduced by Helfrich and Jakobsson [9], who regarded the contact angle as an unknown of the problem, to be determined through minimization arguments. Following a similar line of thought, Nielsen *et al* [15] compared the two approaches but had to conclude that 'at the present time, however, there is insufficient information to establish the appropriate choice of boundary conditions at the bilayer/inclusion boundary' (see p 1977 of [15]).

Also in the most refined models on membrane-induced interactions among proteins, like [4], the Monge gauge has been used systematically to determine the equilibrium shape of a membrane which carries embedded inclusions. As a consequence, the Euler–Lagrange equation which governs the equilibrium turns out to be *linear*. Under this assumption, only membrane configurations which are perturbations of a referential one, be it flat or spherical, can be studied.

Here we consider a *two-dimensional* vesicle formed by a thin bilayer, which is thus modelled as a closed curve, whereas the conical inclusions are modelled as trapezia. The net advantage in doing so is that, although the equilibrium equation is *nonlinear*, we can use a mathematical technique which allows us to obtain the *exact* equilibrium shape of the bilayer, without resort to any linearization near a referential shape. As in the Helfrich–Jakobsson model, we leave the contact angle free to vary. This choice seems plausible in the present context, where closed shapes are sought: more flexibility at the inclusion–membrane interface can help to save energy all along the membrane. Here we introduce an energy penalty for

the values of the contact angle differing from a referential one, which was absent from the Helfrich–Jakobsson model. This approach to the interactions between the membrane and the inclusion, which parallels the treatment of weak anchoring of liquid crystals to a substrate, also reminds us the approach used by Park and Lubensky [16] on dealing with the interactions of a membrane with a nematic inclusion. A further peculiarity of our model is that the direct interactions between the membrane and the inclusion are effective in a region whose size is much smaller than the length of the membrane, so that thickness variations are neglected along the free shape of the membrane.

This paper is organized as follows. In section 2, we deduce through a variational procedure the equilibrium condition at the bilayer–protein interface, when the contact angle is left free to vary. It turns out that this condition involves also the curvature of the membrane at the interface. In section 3, we examine thoroughly the limit case of *strong* anchoring, where the contact angle is frozen. In this case, the equilibrium configurations can be determined analytically: different classes of solutions exist, and we will prove the existence and uniqueness of equilibrium configurations within each class. Our model also accounts for the presence of a non-zero *spontaneous curvature*, and the way in which the inclusion is embedded in the membrane depends on it, yielding a sort of *optimal embedding*, which can be viewed as a counterpart of the results obtained by Dan and Safran [2], where the role of spontaneous curvature in protein conformations was investigated.

Section 4 is devoted to analysis of equilibrium solutions when the anchoring is weak. Though fewer analytical results are available, it is still possible to ascertain the number of equilibrium configurations when both the strength of the constraint and the spontaneous curvature are varied. Several branches of solutions arise and we can determine the energy crossings among them, obtaining, even in this case, a fairly complete characterization of the most efficient way to embed a protein within a membrane. Besides considering the properties of each class of solutions, we will focus our attention on an effect which was absent from the strong anchoring case. It turns out that, when the spontaneous curvature is large enough, regular equilibrium solutions disappear. Of course, amphipathic molecules with extremely high values of the spontaneous curvature are more likely to form micelles rather than vesicles; however, it is important to take care of the lack of regular solutions for reasonable values of the spontaneous curvature. In section 5, we cope with this problem by constructing singular solutions that exhibit self-contact and, hence, have points where the curvature suffers a jump. These solutions tend to *segregate* the protein by forming a neck. This is reminiscent of the behaviour of *coat* proteins, which do really induce a localized increase of the membrane curvature, in order to favour a budding phenomenon [3, 19]. Although it is known [6, 14] that a genuine budding can be properly modelled only in a three-dimensional environment, our results seem to indicate weak anchoring as a simple model to describe the behaviour of coat proteins. Finally, the outcomes of our paper are summarized in section 6.

2. Equilibrium

In this section, we derive the equilibrium equation for the membrane and the boundary conditions arising at the points where a membrane is connected to a rigid, conical inclusion. Using a two-dimensional model, we idealize the membrane as a plane curve γ of length $2L$, and the conical inclusion as a trapezium, with assigned apex angle 2α. The membrane is attached to the protein at two points A and B, whose distance has a fixed value $2a$, as sketched in figure 1. For mathematical completeness, throughout this paper we will allow a to assume values in the whole range $[0, L]$, although we remark that in most cases the ratio a/L ranges from 10^{-3} to 10^{-2} [12]. The height of the inclusion varies 'from the subnano range to many

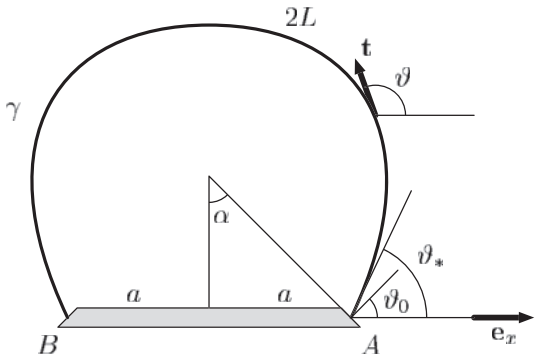

Figure 1. The geometrical setting of our model. The inclusion AB is modelled as a trapezium with lateral sides of length close to $2a$. The height of the membrane can be smaller or larger than the thickness of the membrane bilayer. The configuration of the membrane is identified through the angle ϑ between the tangent $\boldsymbol{t}$ and the unit vector $\boldsymbol{e}_x$, directed along the inclusion.

tens of nanometers' (see p 219 of [12]); it can be either smaller or larger than the membrane thickness, which is usually in the nanometre range: in any case, it plays a minor role in our treatment. The elastic free energy $\mathcal{F}_{\mathrm{e}}$ of the lipid membrane is usually described through a functional which depends at most quadratically on the curvature σ of γ:

$$\mathcal{F}_{\mathrm{e}}[\gamma] := \frac{k}{2}\int_{\gamma}(\sigma-\sigma_0)^2\,\mathrm{d}\ell$$

where the positive constitutive parameter k is referred to as the *bending rigidity* of the membrane, while σ_0 is its *spontaneous curvature*, which reflects the inhomogeneities between the two layers forming the membrane, and $\mathrm{d}\ell$ is the length measure. We recall that, if ϑ is the angle between the unit tangent vector $\boldsymbol{t}$ and the direction $\boldsymbol{e}_x$ (see figure 1), the curvature σ of γ is given by $\sigma = \vartheta'(s)$, where a prime denotes differentiation with respect to the arc length s of γ. In our two-dimensional model, only non-negative values of σ_0 are meaningful. A positive value of σ_0 means that the energetically preferred configuration is a circle of radius $1/\sigma_0$.

2.1. Effective free energy

It is common to impose a *strong* anchoring between the membrane and the inclusion, by requiring them to be mutually orthogonal at the points where they are in contact. Hereafter, we shall refer to such points as the *joint points* of the membrane. In this paper we relax this constraint, by considering a *weak* anchoring, which gives rise to an additional term in the free-energy functional. In fact, we describe the interaction between the inclusion and the membrane through the following anchoring energy, which is a modification of that proposed by Park and Lubensky [16] on studying nematic inclusions:

$$\mathcal{F}_a(\vartheta_*) := -w\cos(\vartheta_*-\vartheta_0) \tag{1}$$

where w is a positive constant measuring the strength of the anchoring, the *contact angle* ϑ_* is simply ϑ evaluated at any joint point such as A in figure 1, and the *preferred angle* ϑ_0 is equal to α when the short side of the inclusion lies inside the membrane (see figure 2(a)), whereas it is equal to $-\alpha$ when the short side of the inclusion lies outside the membrane (see figure 2(b)). Hereafter we will call those sketched in figure 2(a) *inner configurations* and those sketched in figure 2(b) *outer configurations*. Thus, all configurations can be taken into account by considering $\vartheta_0 \in (-\frac{\pi}{2}, \frac{\pi}{2})$. We remark that, though $\mathcal{F}_a$ in (1) does not prescribe the value

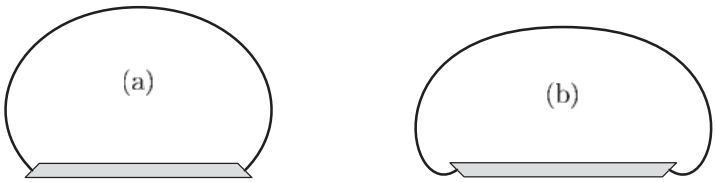

Figure 2. Inner and outer configurations of an inclusion embedded in a membrane.

of ϑ_*, it enhances configurations where $\vartheta_* = \vartheta_0$, especially for high values of w: indeed, strong anchoring is recovered in the limit $w \to +\infty$.

Finally, since the membrane has a fixed length $2L$, we introduce a Lagrange multiplier λ accounting for it. For the sake of simplicity, we will consider only solutions symmetric with respect to the axis of the inclusion, even if our method can be easily modified to account for non-symmetric solutions too. In the class of symmetric solutions the extension Δx of one half of the curve γ must be equal to $-a$ (see figure 1). Taking into account both constraints, the effective free-energy functional we will study is

$$\mathcal{F}_{\text{eff}}[\gamma] := \mathcal{F}_{\text{e}}[\gamma] + \mathcal{F}_a(\vartheta_*) + \lambda \int_\gamma \mathrm{d}s + \mu \int_\gamma \cos\vartheta \, \mathrm{d}s \tag{2}$$

where μ is the Lagrange multiplier associated with the constraint on Δx.

2.2. Equilibrium configurations

To derive both the Euler–Lagrange equation associated with the functional (2) and the boundary conditions to be imposed at the joint points, we perturb a small region surrounding the joint point A, by mapping each point $p(s)$ on γ into a point $p_\varepsilon(s)$ on a new curve γ_ε, according to

$$p(s) \mapsto p_\varepsilon(s) := p(s) + \varepsilon \, \boldsymbol{u}(s) \tag{3}$$

where $\boldsymbol{u}$ is a smooth function with compact support, defined for $s \in [0, L]$. At any point of γ, we expand $\boldsymbol{u}$ in the local basis formed by the unit tangent vector $\boldsymbol{t}$ and the unit normal vector $\boldsymbol{n}$ to γ: $\boldsymbol{u} = u_t \, \boldsymbol{t} + u_n \, \boldsymbol{n}$. Hence, by setting $p(0) = A$, it follows that $\boldsymbol{u}(0) = \boldsymbol{0}$, while $\boldsymbol{u}'(0)$ is left arbitrary. This means that the membrane cannot slide along the inclusion, but it can rotate about the joint point, and so modify the contact angle ϑ_*. The equilibrium conditions are obtained by requiring the functional (2) to be stationary with respect to the perturbations in (3), which is equivalent to setting equal to zero the first variation of $\mathcal{F}_{\text{eff}}$, defined as

$$\delta\mathcal{F}_{\text{eff}} := \left. \frac{\mathrm{d}\, \mathcal{F}_{\text{eff}}[\gamma_\varepsilon]}{\mathrm{d}\varepsilon} \right|_{\varepsilon=0}. \tag{4}$$

To evaluate (4) we need to relate the arc length s_ε and the curvature σ_ε of γ_ε to s and σ, respectively. This is obtained through the following relations (see Virga and Fournier [21]):

$$\frac{\mathrm{d}s_\varepsilon}{\mathrm{d}s} = 1 + \varepsilon \, \boldsymbol{u}' \cdot \boldsymbol{t} + \mathrm{o}(\varepsilon) = 1 + \varepsilon \, (u_t' - \sigma u_n)$$
$$\sigma_\varepsilon = \sigma + \varepsilon \, (v_n' - \sigma v_t)$$

where $v_t := \boldsymbol{u}' \cdot \boldsymbol{t} = u_t' - \sigma \, u_n$, $v_n := \boldsymbol{u}' \cdot \boldsymbol{n} = u_n' + \sigma \, u_t$, and use of the Frénet–Serret formulae has been made.

The angle ϑ is also modified by the perturbation (3): indeed, according to its definition, $\cos\vartheta = \boldsymbol{t} \cdot \boldsymbol{e}_x$, so that $\cos\vartheta_\varepsilon = \boldsymbol{t}_\varepsilon \cdot \boldsymbol{e}_x = \cos\vartheta - \varepsilon \sin\vartheta \, (\boldsymbol{u}' \cdot \boldsymbol{n}) + \mathrm{o}(\varepsilon)$, whence we easily obtain

$\vartheta_\varepsilon - \vartheta = \varepsilon\,(\boldsymbol{u}' \cdot \boldsymbol{n}) + \mathrm{o}(\varepsilon)$. Computing $\mathcal{F}_{\mathrm{eff}}[\gamma_\varepsilon]$, we thus arrive at the following expression for $\delta\mathcal{F}_{\mathrm{eff}}$:

$$\delta\mathcal{F}_{\mathrm{eff}} = \int_\gamma \left[\left(\frac{k}{2}(\sigma - \sigma_0)^2 + \lambda \right) (u_t' - \sigma u_n) + k(\sigma - \sigma_0)\,(v_n' - \sigma v_t) \right] \mathrm{d}s + w \sin(\vartheta_* - \vartheta_0)(\boldsymbol{u}' \cdot \boldsymbol{n}). \tag{5}$$

By integrating by parts in (5), we arrive at the following equilibrium conditions:

$$k\sigma'' - \left(\frac{k}{2}\sigma_0^2 + \lambda \right) \sigma + \frac{k}{2}\sigma^3 = 0 \qquad \text{on} \quad \gamma \tag{6a}$$

$$\sigma(\vartheta_*) = \sigma_0 + \frac{w}{k} \sin(\vartheta_* - \vartheta_0) \qquad \text{at} \quad \mathrm{A}. \tag{6b}$$

Equation (6*a*) is a particular case of the general equilibrium equation already derived, in the context of lipid tubules, by Rosso and Virga [18], while the boundary condition (6*b*) is peculiar to the problem we are dealing with. The multiplier μ does not appear in (6*a*); this is not surprising, since the constraint on Δx is expressed through a null Lagrangian. Moreover, it gives no contribution in (6*b*), since $\boldsymbol{u}$ vanishes at A. Nevertheless, we will see in a moment that this term plays an important role as soon as the equilibrium problem is rephrased in terms of the focal curve f associated with γ. In fact, instead of directly solving the nonlinear differential equation (6*a*), we resort to a geometrical method, introduced in the context of smectic-A liquid crystals by Fournier and Virga [7], and applied to solve two-dimensional problems for lipid membranes in Rosso and Virga [17, 18]. This method rests upon the observation that, whenever a functional defined on a curve has a density $\chi(\vartheta, \sigma)$ which explicitly depends on ϑ and σ, but not on the arc length s, the equilibrium differential equation can be replaced by the following, transcendental one:

$$\sigma \frac{\partial \chi}{\partial \sigma} = \chi. \tag{7}$$

In our case, $\chi(\vartheta, \sigma) = \frac{k}{2}(\sigma - \sigma_0)^2 + \lambda + \mu \cos\vartheta$, and thus the equilibrium equation (6*a*) for the curvature can be replaced by the following one:

$$\sigma^2(\vartheta, \lambda, \mu) = \lambda + \mu \cos\vartheta \tag{8}$$

where, for sake of simplicity, we have still used the symbols λ and μ to denote $\frac{2}{k}\lambda + \sigma_0^2$ and $\frac{2}{k}\mu$, respectively. Equation (8) shows that the curvature σ of the equilibrium curve can change its sign if there is a value $\bar{\vartheta}$ of ϑ which solves the equation $\lambda + \mu \cos\bar{\vartheta} = 0$. Since σ^2 cannot be negative and ϑ has to reach π, solutions with a change of sign in curvature may occur only if $\vartheta \geqslant \bar{\vartheta} > 0$ all along γ. This is equivalent to requiring that the contact angle ϑ_* is positive, that the contact curvature $\sigma(\vartheta_*)$ is negative and that there is precisely one value $\bar{\vartheta} \in (0, \vartheta_*)$ such that $\sigma(\bar{\vartheta}) = 0$. $\bar{\vartheta}$ corresponds to an *inflection point* of γ.

2.3. Constraints

The multipliers λ and μ are determined by imposing the geometric constraints on the length $2L$ of γ, and on Δx. This is equivalent to solving the system

$$L = \int_{\vartheta_*}^{\pi} \frac{\mathrm{d}\vartheta}{\sigma(\vartheta, \lambda, \mu)} \tag{9a}$$

$$a = -\int_{\vartheta_*}^{\pi} \frac{\cos\vartheta\,\mathrm{d}\vartheta}{\sigma(\vartheta, \lambda, \mu)} \tag{9b}$$

if $\sigma(\vartheta, \lambda, \mu)$ is positive all along γ, or

$$\begin{aligned} L &= 2\int_{\bar\vartheta}^{\vartheta_*} \frac{\mathrm{d}\vartheta}{|\sigma(\vartheta,\lambda,\mu)|} + \int_{\vartheta_*}^{\pi} \frac{\mathrm{d}\vartheta}{\sigma(\vartheta,\lambda,\mu)} \\ a &= -2\int_{\bar\vartheta}^{\vartheta_*} \frac{\cos\vartheta\,\mathrm{d}\vartheta}{|\sigma(\vartheta,\lambda,\mu)|} - \int_{\vartheta_*}^{\pi} \frac{\cos\vartheta\,\mathrm{d}\vartheta}{\sigma(\vartheta,\lambda,\mu)} \end{aligned} \tag{10}$$

if $\sigma(\vartheta, \lambda, \mu)$ changes its sign when $\vartheta = \bar\vartheta$.

Finally, the boundary condition (6*b*) determines the value of the contact angle:

$$\sigma(\vartheta_*, \lambda, \mu) = \sigma_0 + \frac{w}{k}\sin(\vartheta_* - \vartheta_0). \tag{11}$$

By combining condition (11) with the foregoing remarks, it is clear that equilibrium solutions with an inflection point may exist only when $0 < \vartheta_* < \vartheta_0$ and

$$w \geqslant \frac{k\,\sigma_0}{\sin\vartheta_0} \tag{12}$$

that is, when the anchoring is sufficiently strong.

3. Strong anchoring

This section is devoted to studying the equilibrium configurations of a membrane when $w \gg \frac{k}{L}$, so that the interaction with the inclusion is strong enough to force the contact angle ϑ_* to coincide with ϑ_0. In this case we will prove that there is a unique equilibrium configuration in the class of inner solutions ($\vartheta_0 > 0$): it solves either (9) or (10) depending on whether ϑ_0 lies below a critical value $\vartheta_{\mathrm{cr}}^{\infty}(\frac{a}{L})$ or not; also in the class of outer solutions ($\vartheta_0 \leqslant 0$) there is a unique equilibrium configuration, and it always solves the system (9). By means of an energetic comparison, we will then ascertain which class contains the minimizer with the lowest free energy, when ϑ_0 and σ_0 are varied.

Firstly, we prove that the system (9) possesses a solution if and only if $\vartheta_0 \in (-\frac{\pi}{2}, \vartheta_{\mathrm{cr}}^{\infty}(\frac{a}{L})]$, where the function $\vartheta_{\mathrm{cr}}^{\infty}$ can be explicitly computed. With this aim, we characterize the region Ω_{ϑ_0} of the (μ, λ)-plane where the function $\sigma(\vartheta, \lambda, \mu)$, satisfying (8), is well defined for all $\vartheta \in [\vartheta_0, \pi]$:

$$\Omega_{\vartheta_0} := \begin{cases} \{(\mu,\lambda) : \lambda - \mu > 0,\ \lambda + \mu > 0\} & \text{if} \quad \vartheta_0 < 0 \\ \{(\mu,\lambda) : \lambda - \mu > 0,\ \lambda + \mu\cos\vartheta_0 > 0\} & \text{if} \quad \vartheta_0 \geqslant 0. \end{cases} \tag{13}$$

The straight line $\mu = 0$ corresponds to circular solutions, regardless of the sign of ϑ_0. It divides Ω_{ϑ_0} in two sets, $\Omega^+_{\vartheta_0}$ and $\Omega^-_{\vartheta_0}$ where μ is positive and negative, respectively. The set $\Omega^+_{\vartheta_0}$ is spanned by straight lines $\lambda = \tau\mu$, whose slope τ lies in the range $(1, +\infty)$. The sign of ϑ_0 affects the size of $\Omega^-_{\vartheta_0}$, since this set is spanned by those straight lines whose slope ranges in $(-\infty, -\cos\vartheta_0)$ when $\vartheta_0 \geqslant 0$ and in $(-\infty, -1)$ otherwise. In any case, the structure of Ω_{ϑ_0} suggests replacing λ by $\tau\mu$, and to describe each point in Ω_{ϑ_0} through the pair (τ, μ). To simplify notations, we define $\varphi(\vartheta, \tau, \mu) := \sigma^{-1}(\vartheta, \tau\mu, \mu)$, and

$$f(\tau,\mu) := \int_{\vartheta_0}^{\pi} \varphi(\vartheta,\tau,\mu)\,\mathrm{d}\vartheta \qquad g(\tau,\mu) := \int_{\vartheta_0}^{\pi} \cos\vartheta\,\varphi(\vartheta,\tau,\mu)\,\mathrm{d}\vartheta.$$

For the sake of brevity, we shall limit our proofs to $\Omega^+_{\vartheta_0}$: only minor changes are needed to repeat the arguments in $\Omega^-_{\vartheta_0}$. For every fixed $\tau > 1$,

$$\lim_{\mu\to 0^+} \varphi(\vartheta,\tau,\mu) = +\infty \qquad \lim_{\mu\to+\infty} \varphi(\vartheta,\tau,\mu) = 0 \qquad \text{and} \qquad \frac{\partial}{\partial\mu}\varphi(\vartheta,\tau,\mu) < 0.$$

Thus, for every assigned value of L, there is a unique value of μ such that $f(\tau, \mu) = L$, as required by (9*a*). Since this argument can be repeated for any choice of $\tau > 1$, we can define a function $\tilde{\mu}$ such that

$$f(\tau, \tilde{\mu}(\tau)) = L. \tag{14}$$

A standard application of the implicit function theorem shows that the function $\tilde{\mu}$ is continuous, decreasing and differentiable. At this stage, we have shown that there are infinitely many values of the multipliers which satisfy (9*a*). To solve the equilibrium problem, we have to ascertain whether the constraint on Δx singles out any of these solutions, and whether a solution exists for any value of a in $[0, L]$. With this aim, we start from a definition.

Definition 3.1. *If $\tilde{\mu}$ satisfies (14) for a fixed value of L, and τ_1 and τ_2 are two real numbers in its domain, we say that the pairs $(\tau_1, \tilde{\mu}(\tau_1))$ and $(\tau_2, \tilde{\mu}(\tau_2))$ are isoperimetric pairs.*

Let us consider two distinct isoperimetric pairs $(\tau_1, \tilde{\mu}(\tau_1))$ and $(\tau_2, \tilde{\mu}(\tau_2))$. They both satisfy (14), so that

$$\int_{\vartheta_0}^{\pi} \varphi(\vartheta, \tau_1, \tilde{\mu}(\tau_1))\, \mathrm{d}\vartheta = \int_{\vartheta_0}^{\pi} \varphi(\vartheta, \tau_2, \tilde{\mu}(\tau_2))\, \mathrm{d}\vartheta.$$

Since the integration domains coincide and both integrands are positive, there exists at least a value $\vartheta_1 \in [\vartheta_0, \pi]$ of ϑ where the integrands coincide. Thus, ϑ_1 satisfies

$$\cos\vartheta_1 = \frac{\tau_2\tilde{\mu}(\tau_2) - \tau_1\tilde{\mu}(\tau_1)}{\tilde{\mu}(\tau_1) - \tilde{\mu}(\tau_2)}. \tag{15}$$

Furthermore, since $\cos\vartheta$ is monotonically decreasing in $[0, \pi]$, such ϑ_1 is unique, if ϑ_0 is not negative. On the other hand, $\cos\vartheta$ being an even function of ϑ, we conclude that, for any $\vartheta_0 \in [-\frac{\pi}{2}, \frac{\pi}{2}]$, equation (15) has at most two opposite solutions. This remark enables us to prove a lemma which essentially states that, if a solution of (9) exists, it is unique. To relieve the presentation, we refer the reader to the appendix for a complete proof.

Lemma 3.1. *Let $(\tau_1, \tilde{\mu}(\tau_1))$ and $(\tau_2, \tilde{\mu}(\tau_2))$ be two distinct isoperimetric pairs. Then*

$$\int_{\vartheta_0}^{\pi} \varphi(\vartheta, \tau_1, \tilde{\mu}(\tau_1)) \cos\vartheta\, \mathrm{d}\vartheta \neq \int_{\vartheta_0}^{\pi} \varphi(\vartheta, \tau_2, \tilde{\mu}(\tau_2)) \cos\vartheta\, \mathrm{d}\vartheta.$$

Lemma 3.1 also shows that

$$\Delta x(\tau) := \int_{\vartheta_0}^{\pi} \varphi(\vartheta, \tau, \tilde{\mu}(\tau)) \cos\vartheta\, \mathrm{d}\vartheta$$

is a monotonic function. Since it is continuous, to show whether it is increasing or decreasing, we only need to know its asymptotic behaviour. We collect the results in the following lemma, which will also be proved in the appendix.

Lemma 3.2. *If $-\frac{\pi}{2} < \vartheta_0 \leqslant 0$, $\lim_{\tau\to 1^+} \Delta x(\tau) = -L$ and $\lim_{\tau\to -1^-} \Delta x(\tau) = L$. On the other hand, if $0 < \vartheta_0 < \frac{\pi}{2}$, $\lim_{\tau\to 1^+} \Delta x(\tau) = -L$ and $\lim_{\tau\to -\cos\vartheta_0} \Delta x(\tau) = h(\vartheta_0)\, L$, where*

$$h(\xi) := \int_{\xi}^{\pi} \frac{\cos\vartheta\, \mathrm{d}\vartheta}{\sqrt{\cos\xi - \cos\vartheta}} \Bigg/ \int_{\xi}^{\pi} \frac{\mathrm{d}\vartheta}{\sqrt{\cos\xi - \cos\vartheta}}.$$

Thus, when $0 < \vartheta_0 < \frac{\pi}{2}$, the constraint $\Delta x(\tau) = -a$ is satisfied if and only if $h(\vartheta_0) \geqslant -\frac{a}{L}$. Figure 3(*a*) shows the graph of h: it is a monotonic function, and so we can define its inverse function $\vartheta_{\mathrm{cr}}^{\infty}(\frac{a}{L})$ (see figure 3(*b*)) in the whole interval $\frac{a}{L} \in [0, 1]$. When ϑ_0 exceeds $\vartheta_{\mathrm{cr}}^{\infty}(\frac{a}{L})$, it is impossible to satisfy the equation $\Delta x(\tau) = -a$. Collecting the results of these lemmas, it is straightforward to prove the following theorem.

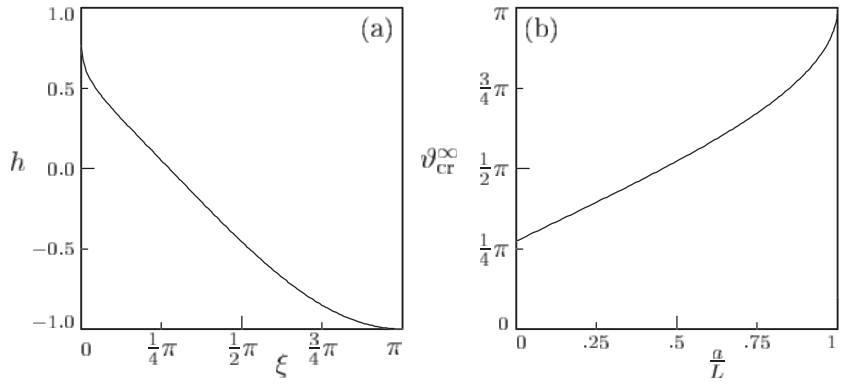

Figure 3. Graphs of the function h defined in the text (*a*), and of its inverse function $\vartheta_{\rm cr}^{\infty}$ (*b*).

Theorem 3.1. *For any $L > 0$ and $a \in [0, L]$, when $\vartheta_0 \in (-\frac{\pi}{2}, \vartheta_{\rm cr}^{\infty}(\frac{a}{L})]$ the system (9) has a unique, symmetric solution, with positive curvature satisfying (8). When $\vartheta_0 > \vartheta_{\rm cr}^{\infty}(\frac{a}{L})$, the system (9) has no solutions.*

When $\vartheta_0 > \vartheta_{\rm cr}^{\infty}$, the system (9) admits no solutions, but this does not mean that the membrane is not able to find an inner equilibrium configuration around the inclusion. In fact, we can still resort to equilibrium configurations which solve system (10), and so have an inflection point. It would be lengthy and cumbersome to repeat for (10) the existence proof we have just worked out for the system (9). Nevertheless, we have accurately studied, also with the aid of numerical methods, the properties of its solutions for many different values of ϑ_0 and $\frac{a}{L} \in [0, 1]$. The conclusions are collected in the following proposition.

Proposition 3.1. *For any $L > 0$ and $a \in [0, L]$, when $\vartheta_0 \in [\vartheta_{\rm cr}^{\infty}(\frac{a}{L}), \frac{\pi}{2})$ the system (10) has a unique, symmetric solution with an inflection point at a value $\bar{\vartheta}(\vartheta_0, \frac{a}{L}) \in (0, \vartheta_0)$, and curvature satisfying (8). When $\vartheta_0 < \vartheta_{\rm cr}^{\infty}(\frac{a}{L})$, the system (10) has no solutions.*

If we now recall that positive values of ϑ_0 describe inner solutions, while negative values describe outer solutions, we can conclude that for any shape of the inclusion there is exactly one inner and exactly one outer equilibrium configuration; furthermore, the inner configuration possesses an inflection point if ϑ_0 is large enough.

It seems plausible that outer configurations, that are characterized by a greater angular excursion, become energetically preferred when the spontaneous curvature σ_0 is large enough, since the only non-trivial contribution of σ_0 to the elastic free energy is given by the term $-k\sigma_0\Delta\vartheta$, where $\Delta\vartheta$ is the total excursion of ϑ along γ. Indeed, computing numerically the energy of both equilibrium solutions, we have found that, for every fixed value of both the apex angle $\alpha = |\vartheta_0|$ and the ratio $\frac{a}{L}$, a critical value $\sigma_0^{\rm cr}$ of the spontaneous curvature exists, such that the absolute minimizer of the free energy is an inner configuration if $\sigma_0 < \sigma_0^{\rm cr}$, while it is an outer configuration if $\sigma_0 > \sigma_0^{\rm cr}$. Figure 4 shows a plot of $\sigma_0^{\rm cr}$ in terms of α for two typical values of the ratio $\frac{a}{L}$. The dots illustrate the values of $\vartheta_{\rm cr}^{\infty}$ above which inner equilibrium configurations exhibit an inflection point. Thus, the way in which the membrane encircles the inclusion suggests a way to estimate the value of the spontaneous curvature σ_0, once α and $\frac{a}{L}$ are known.

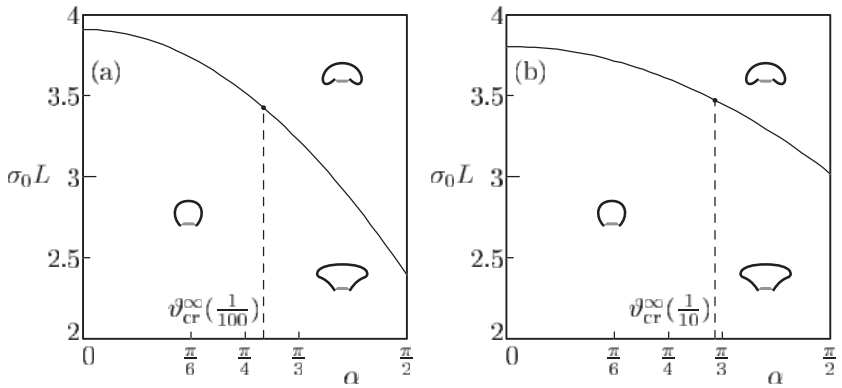

Figure 4. Absolute minimizer of the free energy: in (*a*), $\frac{a}{L} = \frac{1}{100}$; in (*b*), $\frac{a}{L} = \frac{1}{10}$. The optimal embedding of the inclusion changes on crossing the continuous line $\sigma_0^{\mathrm{cr}}(\vartheta_0, \frac{a}{L})$. Inner equilibrium configurations have an inflection point when $\alpha > \vartheta_{\mathrm{cr}}^{\infty}(\frac{a}{L})$.

4. Weak anchoring

As soon as the strong-anchoring condition is relaxed, the uniqueness of the equilibrium configurations within each class is lost: we have to determine the number of equilibrium configurations of the membrane and, among them, the global free energy minimizer.

With this aim, we use the boundary condition (11), to express the multiplier λ in terms of μ and ϑ_*; furthermore, by introducing the dimensionless curvature $\tilde{\sigma} := \sigma L$ and the dimensionless control parameters $\tilde{\sigma}_0 := \sigma_0 L$ and $\tilde{w} := \frac{wL}{k}$, the curvature along the equilibrium solutions can be written as

$$L^2\sigma^2(\vartheta, \vartheta_*, \mu) = \mu(\cos\vartheta - \cos\vartheta_*) + (\tilde{\sigma}_0 + \tilde{w}\sin(\vartheta_* - \vartheta_0))^2 = \tilde{\sigma}^2(\vartheta, \vartheta_*, \mu)$$

where we have mapped $L^2\mu$ into μ without changing the notation.

The multiplier μ and the contact angle ϑ_* must be determined by imposing the geometric constraints on the length $2L$ of γ and on Δx, that is, by solving the system (9) or (10), depending on whether the curvature σ changes its sign or not along the equilibrium curve.

To handle (9), we first note that for any fixed ϑ_* equation (9*a*) has at most two solutions $\mu_i(\vartheta_*)$, $i = 1, 2$, since the function on the right-hand side is convex in μ. Inserting them in (9*b*), we obtain the values of the ratio $\frac{a}{L}$ which allow such a ϑ_* to be an equilibrium value of the contact angle. As a result, uniqueness is lost in most cases and the interplay between the control parameters determines the coexistence of different branches of equilibrium solutions.

Inner and outer equilibrium configurations can be found, as we have shown in the preceding section, by inserting $\vartheta_0 = \pm\alpha$ in the boundary condition (11). Again, outer equilibrium configurations will be preferred when the spontaneous curvature is large enough, but here we will focus our attention on a new feature, characteristic of weak anchoring and common to both classes of configurations. With this aim, we will restrict our study to inner configurations, even if a parallel treatment would yield qualitatively equivalent results for outer configurations.

Let us set $\vartheta_0 = \alpha > 0$. At variance with strong anchoring, solutions with negative curvature are now less likely to occur: not only does condition (12) forbid them if the anchoring energy w is not sufficiently strong but, even if (12) is satisfied, the critical value of ϑ_0 above which they arise is higher, as we state in the following proposition. Its proof can be again found in the appendix.

Proposition 4.1. *Equilibrium shapes with an inflection point can exist in the case of weak*

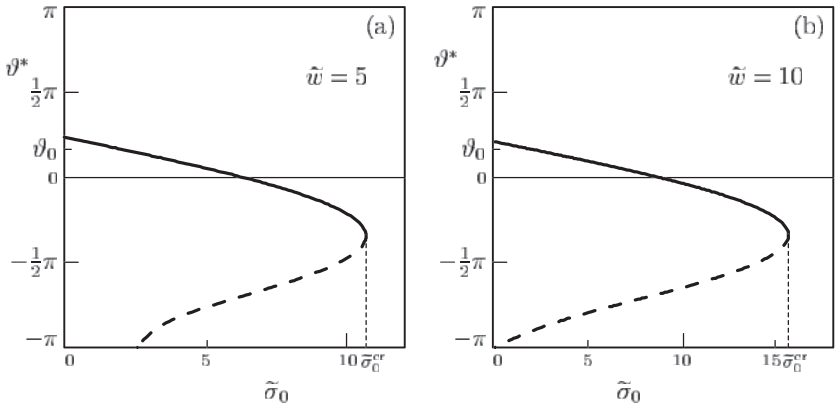

Figure 5. Equilibrium values of ϑ_* for $\vartheta_0 = \frac{\pi}{6}$, $L = 10a$, and $\tilde{w} = 5$ (case (a)) or 10 (case (b)).

anchoring only if $\vartheta_0 \geqslant \vartheta_{\rm cr}^{\rm (weak)}$*, where*

$$\vartheta_{\rm cr}^{\rm (weak)}(a, L, \tilde{w}, \tilde{\sigma}_0) := \vartheta_{\rm cr}^{\infty}\left(\frac{a}{L}\right) + \arcsin\frac{\tilde{\sigma}_0}{\tilde{w}}$$

and $\vartheta_{\rm cr}^{\infty}$ *is the same critical function that allows for the existence of inflection points in the equilibrium shapes, when the anchoring is strong.*

Thus, in particular, these solutions never arise if ϑ_0 is lower than the minimum of $\vartheta_{\rm cr}^{\infty}$. This value is attained when $a \to 0^+$, and it is just greater than $\frac{\pi}{4}$ (see figure 3(b)). In the following, we consider inclusions with $\vartheta_0 < \frac{\pi}{4}$, so that we can concentrate on the study of equilibrium configurations whose curvature is always positive.

To better illustrate the role of the parameters $\tilde{w}$ and $\tilde{\sigma}_0$ in the equilibrium configurations, we initially fix the values of ϑ_0 and $\frac{a}{L}$ to be equal to $\frac{\pi}{6}$ and $\frac{1}{10}$, respectively. If both $\tilde{w}$ and $\tilde{\sigma}_0$ vary, we find situations where there are two, one or even no equilibrium values of the contact angle ϑ_* corresponding to the selected values of the geometric parameters. Figure 5 illustrates how ϑ_* depends on $\tilde{\sigma}_0$ when $\tilde{w}$ is equal to five (figure 5(a)) and ten (figure 5(b)), but qualitatively similar graphs can be found for different values of the anchoring strength. In the figure, the continuous curves denote the absolute minimizer of the free energy, while the dotted curves correspond to unstable equilibrium configurations. It is not surprising that, for any value of $\tilde{\sigma}_0$, the membrane prefers to join the inclusion with the contact angle as close as possible to ϑ_0.

The most surprising feature of figure 5 is the existence of a critical value for the dimensionless parameter $\tilde{\sigma}_0$ above which the membrane is unable to find equilibrium configurations around the inclusion. Since the value $\vartheta_0 = \frac{\pi}{6}$ is not compatible with solutions that exhibit inflection points, this means that the class we have chosen—formed by regular configurations in which the function $\vartheta(s)$ spans an interval $[\vartheta_*, 2\pi - \vartheta_*]$—fails to contain any minimizer of the free energy. Thus, at least when the dimensionless parameter $\sigma_0 L$ is large enough, we have to broaden the class we consider, to include also equilibrium shapes where the curvature suffer jumps at isolated points. We defer a detailed treatment of this topic to the next section; here, we complete the study of weak anchoring by determining how $\tilde{\sigma}_0^{\rm cr}$ depends on $\tilde{w}$, ϑ_0, or $\frac{a}{L}$. Instead of listing the values computed by varying all the external parameters, we just stress that all these results fit (with a relative fitting error of the order of 10^{-3}) into the following functional form:

$$\tilde{\sigma}_0^{\rm cr}\left(\tilde{w}, \vartheta_0, \frac{a}{L}\right) = \tilde{w} + q\left(\vartheta_0, \frac{a}{L}\right). \tag{16}$$

Table 1. Some values of the function $q(\vartheta_0, \frac{a}{L})$ defined in the text.

ϑ_0 \ $q(\vartheta_0, \frac{a}{L})$	0	0.025	0.05	0.075	0.1	0.125	0.15
$\frac{1}{4}\pi$		5.098	5.238	5.409	5.552	5.757	5.945
$\frac{2}{9}\pi$		5.135	5.285	5.443	5.611	5.789	5.976
$\frac{1}{6}\pi$		5.178	5.325	5.484	5.649	5.824	6.010
$\frac{1}{9}\pi$		5.194	5.336	5.487	5.650	5.822	6.005
$\frac{1}{12}\pi$		5.187	5.326	5.476	5.636	5.807	5.988
$\frac{1}{24}\pi$		5.159	5.295	5.441	5.599	5.767	5.946
0							

Table 1 collects some values of $q(\vartheta_0, \frac{a}{L})$. It shows that q increases with the ratio $\frac{a}{L}$ and, as a function of ϑ_0, has a maximum between $\vartheta_0 = \frac{\pi}{9}$ and $\frac{\pi}{6}$. In any case, it always remains in the interval $q \in [5, 6]$ for all the physically reasonable values of ϑ_0 and $\frac{a}{L}$. Clearly, the functional form (16) implies that in the limit $\tilde{w} \to +\infty$ we recover the results we proved in the preceding section: an equilibrium solution exists, regardless of the values of σ_0.

The linear dependence of σ_0^{cr} on w can be explained as follows: σ_0 and w enter explicitly in the expression of the curvature σ through the boundary condition (11); to balance the increasing values of σ_0, the contact angle ϑ_* tends to $\vartheta_0 - \frac{\pi}{2}$ (see figure 5), and the boundary condition on the contact curvature becomes $\tilde{\sigma}_* \simeq \tilde{\sigma}_0 - \tilde{w}$. When this difference exceeds a critical value q, that depends on ϑ_0 and $\frac{a}{L}$, but not on $\tilde{w}$, the contact curvature becomes too large and the membrane is not able to avoid self-contact.

5. Protein segregation

The preceding section has shown that, when the anchoring strength is sufficiently weak and the spontaneous curvature high enough, no regular equilibrium shape exists for the free-energy functional (2). In this section we will enlarge the class of configurations under study in order to better understand the processes that may arise when the spontaneous curvature effects definitely brake the anchoring. In seeking for these new solutions, we are inspired by the behaviour of coat proteins (see [3, 19]), which tend to form buds, by inducing a localized increase in the curvature of the membrane, and so enhance segregation of the protein from the rest of the membrane. Budding is an important step during the processes of *endo-* and *exocytosis*, that serve for transport of material inside or outside a cell. The need for high enough values of the spontaneous curvature to promote budding has been recognized in a similar context by Mashl and Bruinsma [13], for instance.

To segregate a protein from a membrane we can envisage two different processes, which are referred to as the *absorption* (endocytosis) and the *expulsion* (exocytosis) of the protein. To study these singular configurations we allow both adhesion between the protein and the membrane, and self-adhesion of the membrane, as figure 6 shows. We take into account not only the membrane–protein adhesion, but also the self-adhesion of the membrane, in order

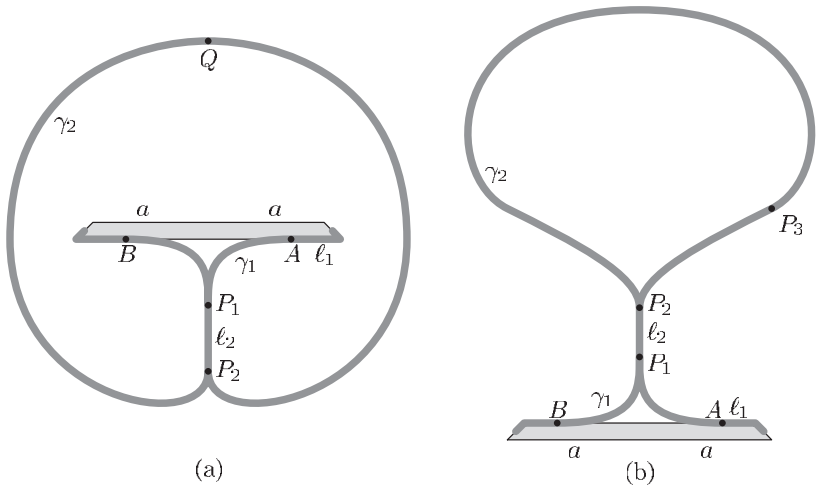

Figure 6. Geometrical settings describing the absorption (*a*) and the expulsion (*b*) of a protein by a membrane.

to describe the final part of the critical processes we are considering, when the protein has been definitely absorbed or expelled by the membrane, even if a similar study would yield (for membranes of smaller length L, as we will show) to configurations exhibiting membrane–protein adhesion, but not self-adhesion.

In the case of absorption (figure 6(*a*)), the membrane adheres to the protein along a segment whose length ℓ_1 is unknown. Then, it has a free segment γ_1 connecting the detachment point A (where $\vartheta(\mathrm{A}) = -\pi$) to the self-adhesion point P_1, where $\vartheta(\mathrm{P}_1) = -\frac{\pi}{2}$. The equilibrium curvature σ_1 of γ_1 has the usual analytical expression

$$L\sigma_1(\vartheta) = \sqrt{\lambda_1 + \mu_1 \cos\vartheta} \qquad \text{with} \quad \vartheta \in \left[-\pi, -\frac{\pi}{2}\right] \tag{17}$$

where λ_1 and μ_1 will be determined by imposing suitable detachment conditions. At P_1, the membrane has a self-adhesion segment of unknown length ℓ_2, which ends at P_2, whence the free segment γ_2 starts; its curvature σ_2 is given by

$$L\sigma_2(\vartheta) = \sqrt{\lambda_2 + \mu_2 \cos\vartheta} \qquad \text{with} \quad \vartheta \in \left[-\frac{\pi}{2}, \pi\right]. \tag{18}$$

A similar description holds also in the case of expulsion (figure 6(*b*)). The membrane detaches from the protein at a point A where $\vartheta(\mathrm{A}) = \pi$, and exhibits self-adhesion along a segment $\mathrm{P}_1\mathrm{P}_2$ of length ℓ_2, where $\vartheta \equiv \frac{\pi}{2}$. These shapes always have two inflection points along γ_2: in figure 6(*b*), they are the point P_3 and its symmetric point with respect to the axis of the protein.

To study both classes of configurations we have to insert in the free-energy functional two further contributions arising from the adhesion and self-adhesion potentials. Thus, we have to consider the following modified free-energy functional:

$$\mathcal{F}[\gamma] := \frac{k}{2}\int_\gamma (\sigma - \sigma_0)^2 \,\mathrm{d}\ell - \beta\,\ell_1 - \delta\,\ell_2 \tag{19}$$

where β and δ respectively denote the membrane–protein adhesion potential and the self-adhesion potential of the membrane. The curve γ is the union of the free curves γ_1 and γ_2 and

the adhering segments of length ℓ_1 and ℓ_2. At any detachment point, the curvature suffers a jump passing from zero to the values σ_β or σ_δ which verify [20]

$$\sigma_\beta^2 = \frac{2\beta}{k} \qquad \text{and} \qquad \sigma_\delta^2 = \frac{2\delta}{k} \tag{20}$$

depending on whether we are considering adhesion to the protein or self-adhesion, respectively. By replacing the free-energy functional (1) with (19), we want to stress the role of both weak anchoring and spontaneous curvature to promote singular solutions: absorption and expulsion are forbidden if strong anchoring is enforced, since they both require the contact angle ϑ_* to assume values rather far from the preferred angle ϑ_0; furthermore, in the preceding section we have shown that ϑ_* departs significantly from ϑ_0 only when the spontaneous curvature is high enough. When this is the case, more complicated interactions arise at the membrane–protein interface; we model them by inserting adhesion contributions in the free-energy functional, but it should be noticed that the adhesion potential β will depend in general both on the anchoring strength w and on the spontaneous curvature σ_0. In a three-dimensional setting, where budding phenomena can be described more properly, a complete treatment of the boundary conditions to be imposed when a neck is formed in a two-component vesicle can be found in the paper by Jülicher and Lipowsky [11].

5.1. Absorption

The boundary condition (20) can be used to relate the Lagrange multipliers to the adhesion potentials. In fact, by use of (17) and (18) we obtain

$$\begin{array}{l} \lambda_1 - \mu_1 = L^2\sigma_\beta^2 \quad \text{(equil. at } A\text{)} \\ \lambda_1 = \lambda_2 = L^2\sigma_\delta^2 \quad \text{(equil. at P}_1 \text{ and P}_2\text{)} \end{array} \Longrightarrow \begin{cases} \lambda_1 = L^2\sigma_\delta^2 \\ \mu_1 = \nu_1\, L^2\sigma_\delta^2 \\ \lambda_2 = L^2\sigma_\delta^2 \end{cases}$$

$$\text{where} \quad \nu_1 := 1 - \left(\frac{\sigma_\beta}{\sigma_\delta}\right)^2 < 1.$$

Moreover, we determine μ_2 by setting equal to zero the total horizontal excursion of the curve γ_2:

$$\int_{-\frac{\pi}{2}}^{\pi} \frac{\cos\vartheta\,\mathrm{d}\vartheta}{\sqrt{\lambda_2 + \mu_2\cos\vartheta}} = 0 \Longrightarrow \mu_2 = \nu_2\, L^2\sigma_\delta^2 \qquad \text{with} \quad \nu_2 \simeq 0.73.$$

The lengths of the adhering segments ℓ_1 and ℓ_2 can be retrieved as functions of σ_β and σ_δ by use of the constraints on the total length of the membrane and the horizontal excursion of γ_1:

$$\begin{aligned} \ell_1 &= a + L\int_{-\pi}^{-\frac{\pi}{2}} \frac{\cos\vartheta\,\mathrm{d}\vartheta}{\sqrt{\lambda_1 + \mu_1\cos\vartheta}} = a - \frac{1}{\sigma_\delta}\int_0^{\frac{\pi}{2}} \frac{\cos\vartheta\,\mathrm{d}\vartheta}{\sqrt{1-\nu_1\cos\vartheta}} \\ \ell_2 &= L - \ell_1 - L\int_{-\pi}^{-\frac{\pi}{2}} \frac{\mathrm{d}\vartheta}{\sqrt{\lambda_1 + \mu_1\cos\vartheta}} - L\int_{-\frac{\pi}{2}}^{\pi} \frac{\mathrm{d}\vartheta}{\sqrt{\lambda_2 + \mu_2\cos\vartheta}} \\ &= L - a - \frac{1}{\sigma_\delta}\left(\int_0^{\frac{\pi}{2}} \frac{(1-\cos\vartheta)\,\mathrm{d}\vartheta}{\sqrt{1-\nu_1\cos\vartheta}} + c_1\right) \end{aligned} \tag{21}$$

where $c_1 := \int_{-\frac{\pi}{2}}^{\pi} \frac{\mathrm{d}\vartheta}{\sqrt{1+\nu_2\cos\vartheta}} \simeq 7.21$.

It is clear from (21) that the adhesion lengths ℓ_1 and ℓ_2 are always smaller than a and L, respectively, as it should be, but, in addition, they must also be positive: this constraint restricts the admissible values of the adhesion potentials δ, β, which have to satisfy

$$\frac{1}{\sigma_\delta}\int_0^{\frac{\pi}{2}} \frac{\cos\vartheta}{\sqrt{1-\nu_1\cos\vartheta}}\,\mathrm{d}\vartheta \leqslant a \qquad \text{and} \qquad \frac{1}{\sigma_\delta}\left(\int_0^{\frac{\pi}{2}} \frac{(1-\cos\vartheta)}{\sqrt{1-\nu_1\cos\vartheta}}\,\mathrm{d}\vartheta + c_1\right) \leqslant L - a.$$

(22)

When the former condition is not satisfied, the adhesion potential is not sufficiently strong to break the anchoring; on the other hand, if the latter condition fails, the anchoring is broken and the membrane adheres to the protein, but it is not able to self-adhere in order to complete the absorption process.

Moreover, a glance at figure 6(*a*) should suffice to convince us that an equilibrium solution is meaningful only when the point Q is above the protein. Denoting by Δy_1 and Δy_2 the vertical excursions of the curves γ_1 and γ_2, this amounts to requiring that $\Delta y_1 - \ell_2 + \Delta y_2 \geqslant 0$ or, in terms of σ_δ and $\nu_1 = 1 - (\sigma_\beta/\sigma_\delta)^2$,

$$\frac{1}{\sigma_\delta}\left(\int_0^{\frac{\pi}{2}} \frac{1-\cos\vartheta-\sin\vartheta}{\sqrt{1-\nu_1\cos\vartheta}}\,\mathrm{d}\vartheta + c_1 + c_2\right) \geqslant L - a \tag{23}$$

where $c_2 := \int_{-\frac{\pi}{2}}^{\pi} \frac{\sin\vartheta\,\mathrm{d}\vartheta}{\sqrt{1+\nu_2\cos\vartheta}} = \frac{2}{\nu_2}(1-\sqrt{1-\nu_2}) \simeq 1.32$.

Let us introduce the scaled curvatures $\tilde\sigma_\delta := L\sigma_\beta$ and $\tilde\sigma_\beta := L\sigma_\beta$. Figure 7 shows the region of the $(\tilde\sigma_\delta, \tilde\sigma_\beta)$-plane where all the constraints (22) and (23) are satisfied. When the pair $(\tilde\sigma_\delta, \tilde\sigma_\beta)$ lies below the curve labelled as I, the membrane cannot adhere to the protein and the anchoring is not broken. In the region above the curve I but on the left of the curve II, the membrane adheres to the protein but it does not complete the absorption process; we remark that, given any value of $(\tilde\sigma_\delta, \tilde\sigma_\beta)$ in this region, it is possible to complete the absorption process by increasing sufficiently the length L of the membrane, that increases linearly both scaled curvatures, yielding them to the grey region. Finally, if $(\tilde\sigma_\delta, \tilde\sigma_\beta)$ lies on the right of the curve III, the self-adhesion potential is so strong that the membrane cannot close itself above the protein.

5.2. Expulsion

Exactly as in the case of absorption, the detachment condition (20) determines the Lagrange multipliers that characterize the free parts of the membrane; again we obtain

$$\lambda_1 = \lambda_2 = \tilde\sigma_\delta^2 \qquad \text{and} \qquad \mu_1 = \nu_1\,\tilde\sigma_\delta^2 \qquad \text{with} \quad \nu_1 := 1 - \left(\frac{\sigma_\beta}{\sigma_\delta}\right)^2 < 1.$$

The remaining coefficient μ_2 is related to the angle $\bar\vartheta \in (0, \frac{\pi}{2})$, corresponding to the point P_3, where the membrane has an inflection point (see figure 6(*b*)):

$$L^2\sigma_2^2(\bar\vartheta) = \tilde\sigma_\delta^2 + \mu_2\cos\bar\vartheta = 0 \Longrightarrow \mu_2 = -\frac{\tilde\sigma_\delta^2}{\cos\bar\vartheta}.$$

Finally, to determine $\bar\vartheta$ we impose that the total horizontal excursion of γ_2 must vanish:

$$2\int_{\bar\vartheta}^{\frac{\pi}{2}} \frac{\cos\vartheta\,\mathrm{d}\vartheta}{\sqrt{\cos\bar\vartheta-\cos\vartheta}} + \int_{\frac{\pi}{2}}^{\pi} \frac{\cos\vartheta\,\mathrm{d}\vartheta}{\sqrt{\cos\bar\vartheta-\cos\vartheta}} = 0 \Longrightarrow \bar\vartheta \simeq 1.09\ \text{rad} \approx 62.46^\circ.$$

The lengths ℓ_1 and ℓ_2 can again be obtained by imposing the constraints on the total length of the membrane and the horizontal excursion of γ_1:

$$\ell_1 = a - \frac{1}{\sigma_\delta}\int_0^{\frac{\pi}{2}} \frac{\cos\vartheta\,\mathrm{d}\vartheta}{\sqrt{1-\nu_1\cos\vartheta}}$$

$$\ell_2 = L - a - \frac{1}{\sigma_\delta}\left(\int_0^{\frac{\pi}{2}} \frac{(1-\cos\vartheta)\,\mathrm{d}\vartheta}{\sqrt{1-\nu_1\cos\vartheta}} + c_3\right)$$

where

$$c_3 := \sqrt{\cos\bar\vartheta}\left(2\int_{\bar\vartheta}^{\frac{\pi}{2}} \frac{\mathrm{d}\vartheta}{\sqrt{\cos\bar\vartheta-\cos\vartheta}} + \int_{\frac{\pi}{2}}^{\pi} \frac{\mathrm{d}\vartheta}{\sqrt{\cos\bar\vartheta-\cos\vartheta}}\right) \simeq 3.03.$$

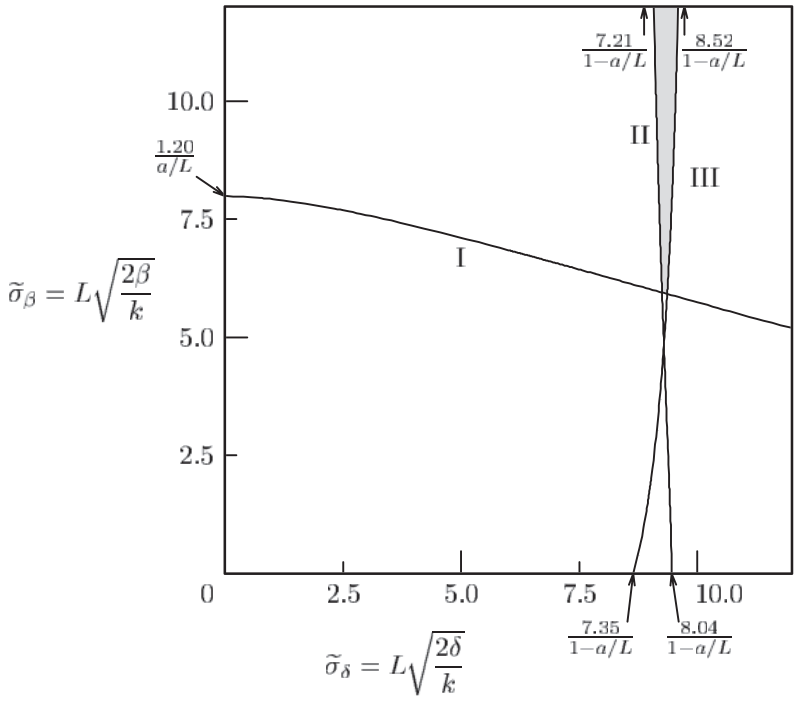

Figure 7. Phase diagram concerning protein absorption. The grey region contains the values of the scaled curvatures $(\tilde{\sigma}_\delta, \tilde{\sigma}_\beta)$ for which absorption is possible. The graphs have been drawn taking $a = 0.15L$, but the outcomes are similar when the protein size is changed. The points where curves I, II and III intersect the axes depend only on $\frac{a}{L}$. A similar remark holds for the asymptotic values of curves II and III.

The conditions ensuring that ℓ_1 and ℓ_2 are positive now become

$$\frac{1}{\sigma_\delta}\int_0^{\frac{\pi}{2}} \frac{\cos\vartheta\,\mathrm{d}\vartheta}{\sqrt{1-\nu_1\cos\vartheta}} \leqslant a \qquad \text{and} \qquad \frac{1}{\sigma_\delta}\left(\int_0^{\frac{\pi}{2}} \frac{(1-\cos\vartheta)\,\mathrm{d}\vartheta}{\sqrt{1-\nu_1\cos\vartheta}} + c_3\right) \leqslant L - a.$$

Figure 8 illustrates the region in the $(\tilde{\sigma}_\delta, \tilde{\sigma}_\beta)$-plane where both conditions are satisfied: if $\tilde{\sigma}_\delta$ lies below the curve I, the adhesion potential is not able to ensure the adhesion between the membrane and the protein; on the other hand, when $\tilde{\sigma}_\delta$ lies on the left side of curve II, the self-adhesion potential cannot sustain the self-adhesion of the membrane.

On comparing the phase diagrams shown in figures 7 and 8, we see that absorption is possible when $\tilde{\sigma}_\beta$ is greater than a minimum value, with $\tilde{\sigma}_\delta$ ranging between a minimum and a maximum value. On the other hand, the expulsion is more likely to occur, since it only requires that both $\tilde{\sigma}_\beta$ and $\tilde{\sigma}_\delta$ must exceed a minimum value: for any value of both the adhesion and the self-adhesion potentials, there exists a minimum value of the length L of the membrane above which the expulsion of the protein becomes possible. As an aside, we note that the location of curve I depends only on the ratio $\frac{a}{L}$, and it is the same for both the absorption and the expulsion.

When both expulsion and absorption are allowed, an energetic comparison is needed to ascertain which process is more favourable. As a result we have found that expulsion is preferred when the spontaneous curvature σ_0 is below a critical value σ_0^{cr}, whereas absorption is favoured when $\sigma_0 > \sigma_0^{\mathrm{cr}}$. If fact, since both the shape of the free curves and the length of the adhering segments depend only on $\tilde{\sigma}_\delta$ and $\tilde{\sigma}_\beta$, the free energy of both solutions can be written

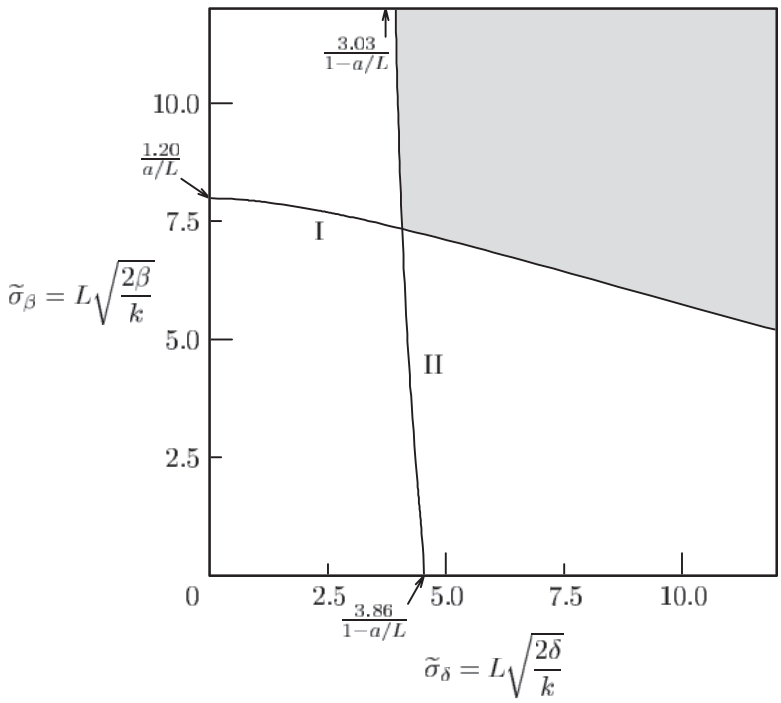

Figure 8. Phase diagram concerning protein expulsion. Expulsion is possible only when the dimensionless parameters $\tilde{\sigma}_\delta$ and $\tilde{\sigma}_\beta$ lie in the grey region. The graphs have been drawn taking $a = 0.15L$, but the outcomes are similar when the protein size is changed. As in figure 7, both the intersections of the curves with the axes and the asymptotic value of curve II depend only upon $\frac{a}{L}$.

as

$$\mathcal{F}_{e,\mathrm{adh}} = \frac{k}{2L}[\sigma_0^2 L^2 - 2\,\sigma_0 L\,\Delta\vartheta + f(\tilde{\sigma}_\delta, \tilde{\sigma}_\beta))]$$

$$\text{where} \quad \Delta\vartheta = \begin{cases} 0 & \text{in the case of expulsion} \\ 2\pi & \text{in the case of absorption} \end{cases}$$

and the function f depends on the type of solution we are considering. Thus, the critical value of $\sigma_0 L$ is given by

$$\sigma_0^{\mathrm{cr}} L = \frac{f_{\mathrm{abs}}(\tilde{\sigma}_\delta, \tilde{\sigma}_\beta) - f_{\mathrm{exp}}(\tilde{\sigma}_\delta, \tilde{\sigma}_\beta)}{4\pi}.$$

6. Concluding remarks

The preferred arrangement of the membrane around an embedded, rigid inclusion and the behaviour of its curvature yield information on the constitutive parameters characterizing both the membrane and the way it interacts with the inclusion. In particular, if the ratio $\frac{a}{L}$ between the lengths of the inclusion and the membrane and the angle ϑ_0 characterizing the shape of the membrane are known, it is possible to estimate either the spontaneous curvature σ_0 of the membrane or the strength w of the anchoring between the membrane and the inclusion.

When the anchoring is so strong that the contact angle ϑ_* is fixed, we have proved that there are two equilibrium configurations for the membrane. In the former, the *inner* solution,

the total excursion of the angle ϑ is lower than 2π; furthermore, this solution exhibits an inflection point if ϑ_0 exceeds a critical value. In the latter, the *outer* solution, $\Delta\vartheta$ is greater than 2π. Moreover, we have proved that it provides the absolute minimizer if the spontaneous curvature exceeds a critical threshold, as it is natural to expect, since greater angular excursions allow the membrane to lower its free energy.

The situation is more complex when the anchoring strength w is finite. First of all, even in each class of solutions, the equilibrium configuration fails to be unique. More interestingly, there is still another critical value of the spontaneous curvature above which no minimizer of the free-energy function can be found, without self-contact. In section 4 we have shown that this value increases linearly with w, and we have determined its dependence on ϑ_0 and $\frac{a}{L}$. To cure the absence of regular equilibrium configurations, we have envisaged two different processes through which the protein is segregated from the membrane. The weak anchoring promotes the formation of these configurations which are controlled by the phenomenological adhesion potentials β and δ. It is again the value of the spontaneous curvature to decide which kind of segregation is the most advantageous, either expulsion or absorption.

Acknowledgments

It is a pleasure to acknowledge Professor Epifanio G Virga, for useful discussions and comments. This paper was made possible by the post-doctoral fellowship 'Mathematical models for fluid membranes', supported by the Mathematical Department of the *Politecnico di Milano*.

Appendix

Proof of lemma 3.1. Let us define

$$\Delta x(\tau) := \int_{\vartheta_0}^{\pi} \varphi(\vartheta, \tau, \tilde{\mu}(\tau)) \cos\vartheta \, \mathrm{d}\vartheta.$$

An integration by parts yields

$$\Delta x(\tau) = -\int_{\vartheta_0}^{\pi} \varphi(\vartheta, \tau, \tilde{\mu}(\tau)) \, \mathrm{d}\vartheta + \int_{\vartheta_0}^{\pi} \sin\vartheta L(\vartheta, \tau) \, \mathrm{d}\vartheta = -L + \int_{\vartheta_0}^{\pi} \sin\vartheta L(\vartheta, \tau) \, \mathrm{d}\vartheta \quad \text{(A1)}$$

where we have noted that $L(\vartheta, \tau) := \int_{\vartheta_0}^{\vartheta} \varphi(\xi, \tau, \tilde{\mu}(\tau)) \, \mathrm{d}\xi$ is the length of the arc of γ, where the angle formed by the unit tangent vector and $\boldsymbol{e}_x$ ranges from ϑ_0 to ϑ. By (15), if $\vartheta_0 \geqslant 0$, $\varphi(\vartheta, \tau_1, \tilde{\mu}(\tau_1))$ and $\varphi(\vartheta, \tau_2, \tilde{\mu}(\tau_2))$ intersect only once when $\vartheta \in [\vartheta_0, \pi]$, as shown in figure A1($a$). The dashed regions in figure A1(a) must have the same area, since we are considering isoperimetric pairs and this, in turn, implies that for any $\vartheta < \pi$ the functions $L(\vartheta, \tau_1)$ and $L(\vartheta, \tau_2)$ must have different values. Thus

$$\Delta x(\tau_1) - \Delta x(\tau_2) = \int_{\vartheta_0}^{\pi} \sin\vartheta [L(\vartheta, \tau_1) - L(\vartheta, \tau_2)] \, \mathrm{d}\vartheta \neq 0 \quad \text{(A2)}$$

which proves the lemma when $\vartheta_0 \geqslant 0$. When ϑ_0 is negative, the most delicate situation we might encounter is shown in figure A1(b). Here again, the areas below the functions $\varphi(\vartheta, \tau_1, \tilde{\mu}(\tau_1))$ and $\varphi(\vartheta, \tau_2, \tilde{\mu}(\tau_2))$ must coincide. Let us introduce the angle ϑ_e, which satisfies

$$\int_{\vartheta_0}^{\vartheta_e} [\varphi(\vartheta, \tau_1, \tilde{\mu}(\tau_1)) - \varphi(\vartheta, \tau_2, \tilde{\mu}(\tau_2))] \, \mathrm{d}\vartheta = 0.$$

Since we are considering isoperimetric pairs, and φ is an even function of ϑ, ϑ_e cannot be positive. The function $L(\vartheta, \tau_1) - L(\vartheta, \tau_2)$ has the graph sketched in figure A1(c), whence it

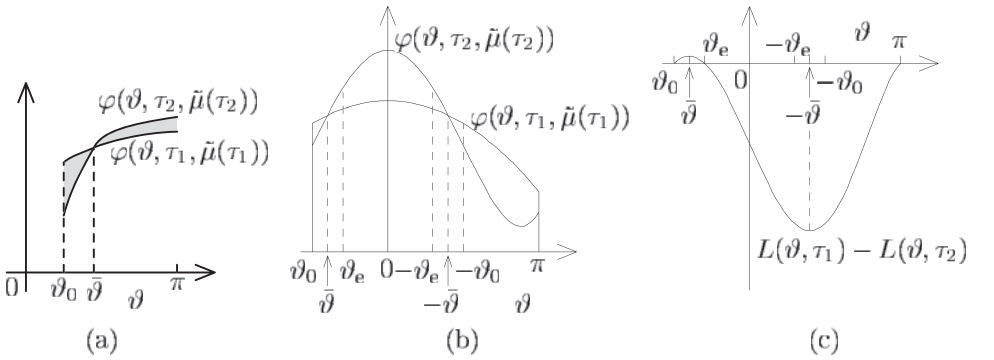

Figure 9. The graphs represent, respectively, the functions $\varphi(\vartheta,\tau_i,\tilde\mu(\tau_i))$, for $i=1,2$, when ϑ_0 is positive (*a*), and negative (*b*). In this latter case, the graph of the difference $L(\vartheta,\tau_1)-L(\vartheta,\tau_2)$ is also shown (*c*).

follows that the integrand in (A2) is negative when ϑ ranges in $[\vartheta_0,\vartheta_e]\cup[-\vartheta_e,\pi]$. In the remaining set $[\vartheta_e,-\vartheta_e]$, $\sin\vartheta$ being an odd function of ϑ, it turns out that

$$\int_{\vartheta_e}^{-\vartheta_e}\sin\vartheta[L(\vartheta,\tau_1)-L(\vartheta,\tau_2)]\,\mathrm{d}\vartheta<0$$

which proves the lemma also in the case when ϑ_0 is negative. In the proof, it was tacitly assumed that both τ_1 and τ_2 belong to $\Omega^+_{\vartheta_0}$. It is easy to adapt the proof to deal with the other possibilities. □

Proof of lemma 3.2. We begin by proving that $\tilde\mu$ diverges when $\tau\to1^+$. The function $\tilde\mu$ is monotonically decreasing, so the limits we are seeking certainly exist. We can write (14) as

$$\frac{1}{\sqrt{|\tilde\mu(\tau)|}}\int_{\vartheta_0}^{\pi}\frac{\mathrm{d}\vartheta}{\sqrt{|\tau+\cos\vartheta|}}=L \tag{A3}$$

since the integrand has a non-integrable singularity as $\tau\to1^+$, in this limit $\tilde\mu(\tau)$ must diverge. As an aside, we note that $\tilde\mu(\tau)$ must tend to zero as $\tau\to\pm\infty$, since otherwise (A3) would not be satisfied: the structure of (A3) ensures that $\tilde\mu(\tau)=\mathrm{O}(\tau^{-1})$ when $\tau\to\pm\infty$. Let us consider the case when $\vartheta_0\leqslant0$. In the limit when $\tau\to-1^-$, the integral in (A3) is again singular, and it is possible to show that $\tilde\mu\to-\infty$, by repeating the arguments just used. As to Δx, we can always write

$$\Delta x(\tau)=\frac{1}{\sqrt{|\tilde\mu(\tau)|}}\int_{\vartheta_0}^{\pi}\frac{1+\cos\vartheta}{\sqrt{|\tau+\cos\vartheta|}}\,\mathrm{d}\vartheta-L$$

and so, when $\tau\to1^+$, we have

$$\lim_{\tau\to1^+}\Delta x(\tau)=-L \tag{A4}$$

because of the asymptotic behaviour of $\tilde\mu$. Similarly,

$$\Delta x(\tau)=L-\frac{1}{\sqrt{|\tilde\mu(\tau)|}}\int_{\vartheta_0}^{\pi}\frac{1-\cos\vartheta}{\sqrt{|\tau+\cos\vartheta|}}\,\mathrm{d}\vartheta$$

whence it follows that

$$\lim_{\tau\to-1^-}\Delta x(\tau)=L.$$

When $\vartheta_0 > 0$ (A4) still holds, but, since the integral in (A3) is convergent when $\tau \to -\cos\vartheta_0$, we can no longer conclude that $\lim_{\tau\to-\cos\vartheta_0}\tilde{\mu}(\tau) = -\infty$: indeed,

$$\lim_{\tau\to-\cos\vartheta_0}\tilde{\mu}(\tau) = -\left(\frac{1}{L}\int_{\vartheta_0}^{\pi}\frac{\mathrm{d}\vartheta}{\sqrt{\cos\vartheta_0-\cos\vartheta}}\right)^2.$$

Thus,

$$\lim_{\tau\to-\cos\vartheta_0}\Delta x(\tau) = L\frac{\int_{\vartheta_0}^{\pi}\frac{\cos\vartheta\,\mathrm{d}\vartheta}{\sqrt{\cos\vartheta_0-\cos\vartheta}}}{\int_{\vartheta_0}^{\pi}\frac{\mathrm{d}\vartheta}{\sqrt{\cos\vartheta_0-\cos\vartheta}}} =: L\,h(\vartheta_0)$$

so $\Delta x(\tau)$ spans the interval $[-L, L\,h(\vartheta_0)]$, and the equation $\Delta x(\tau) = -a$ has a solution if and only if $h(\vartheta_0) \geqslant -\frac{a}{L}$. □

Proof of proposition 4.1. Using equations (10), and the fact that the inflection angle $\bar{\vartheta}$ satisfies the condition $\lambda + \mu\cos\bar{\vartheta} = 0$, we obtain that, for any value of ϑ_*, the angle $\bar{\vartheta}$ must solve the equation

$$j(\bar{\vartheta}) := \frac{2\int_{\bar{\vartheta}}^{\vartheta_*}\frac{\cos\vartheta\,\mathrm{d}\vartheta}{\sqrt{\cos\bar{\vartheta}-\cos\vartheta}} + \int_{\vartheta_*}^{\pi}\frac{\cos\vartheta\,\mathrm{d}\vartheta}{\sqrt{\cos\bar{\vartheta}-\cos\vartheta}}}{2\int_{\bar{\vartheta}}^{\vartheta_*}\frac{\mathrm{d}\vartheta}{\sqrt{\cos\bar{\vartheta}-\cos\vartheta}} + \int_{\vartheta_*}^{\pi}\frac{\mathrm{d}\vartheta}{\sqrt{\cos\bar{\vartheta}-\cos\vartheta}}} = -\frac{a}{L} \qquad \text{with} \quad \bar{\vartheta} \in (0, \vartheta_*). \tag{A5}$$

When $\bar{\vartheta} \to 0^+$, the former integrals in both the numerator and the denominator diverge, and

$$\lim_{\bar{\vartheta}\to 0^+} j(\bar{\vartheta}) = 1$$

since the divergence occurs near $\vartheta = 0$, where $\cos\vartheta$ tends to 1. On the other hand, when $\bar{\vartheta}$ approaches ϑ_*, the same integrals tend to zero, and

$$\lim_{\bar{\vartheta}\to\vartheta_*} j(\bar{\vartheta}) = h(\vartheta_*)$$

where h is the function that was introduced in lemma 3.2, and plotted in figure 3(*a*). It is as lengthy to prove analytically as immediate to check it numerically that j is a monotonically decreasing function. Thus, there exists one (and precisely one) solution to (A5) if and only if

$$h(\vartheta_*) \leqslant -\frac{a}{L}. \tag{A6}$$

Now, h is a monotonically decreasing function in $(0, \pi)$, with $\lim_{x\to0^+} h(x) = 1$ and $\lim_{x\to\pi^-} h(x) = -1$, but ϑ_* is forced to lie in the interval $(0, \vartheta_0 - \arcsin\frac{\tilde{\sigma}_0}{\tilde{w}})$ in order to ensure a negative contact curvature σ_*. Thus, condition (A6) becomes

$$h\left(\vartheta_0 - \arcsin\frac{\tilde{\sigma}_0}{\tilde{w}}\right) \leqslant -\frac{a}{L}$$

which, inverted, yields

$$\vartheta_0 - \arcsin\frac{\tilde{\sigma}_0}{\tilde{w}} \geqslant h^{-1}\left(-\frac{a}{L}\right) = \vartheta_{\mathrm{cr}}^{\infty}\left(\frac{a}{L}\right)$$

that is the desired result. □

References

[1] Dan N, Berman A, Pincus P and Safran A 1994 Membrane-induced interactions between inclusions *J. Physique* I **4** 1713–25

[2] Dan N and Safran S A 1998 Effect of lipid characteristics on the structure of transmembrane proteins *Biophys. J.* **75** 1410–4

[3] De Camilli P, Emr S D, McPherson P S and Novick P 1996 Phosphoinositides as regulators in membrane traffic *Science* **271** 1533–9

[4] Dommersnes P G and Fournier J-B 1999 N-body study of anisotropic membrane inclusions. Membrane mediated interactions and ordered aggregation *Eur. Phys. J.* B **12** 9–12

[5] Dommersnes P G, Fournier J-B and Galatola P 1998 Long-range elastic forces between membrane inclusions in spherical vesicles *Europhys. Lett.* **42** 233–8

[6] Fourcade B, Miao L, Rao M and Wortis M 1994 Scaling analysis of narrow necks in curvature models of fluid lipid-bilayer vesicles *Phys. Rev.* E **49** 5276–86

[7] Fournier J-B and Virga E G 1996 Geometrical exact solutions for confocal lamellar textures yielding confinement and faceting phenomena *Proc. R. Soc.* A **452** 1251–61

[8] Goulian M, Bruinsma R and Pincus R 1993 Long-range forces in heterogeneous fluid membranes *Europhys. Lett.* **22** 145–50

[9] Helfrich P and Jakobsson E 1990 Calculation of deformation energies and configurations in lipid membranes containing gramicidin channels *Biophys. J.* **57** 1057–84

[10] Jähnig F 1996 What is the surface tension of a lipid bilayer membrane? *Biophys. J.* **71** 1348–9

[11] Jülicher F and Lipowsky R 1996 Shape transformations of vesicles with intramembrane domains *Phys. Rev.* E **53** 2670–83

[12] Lipowsky R and Döbereiner H-G 1998 Vesicles in contact with nanoparticles and colloids *Europhys. Lett.* **43** 219–25

[13] Mashl R J and Bruinsma R F 1998 Spontaneous-curvature theory of clathrin-coated membranes *Biophys. J.* **74** 2862–75

[14] Miao L, Fourcade B, Rao M and Wortis M 1991 Equilibrium budding and vesiculation in the curvature model of fluid lipid membranes *Phys. Rev.* A **43** 6843–56

[15] Nielsen C, Goulian M and Andersen O S 1998 Energetics of inclusion-induced bilayer deformations *Biophys. J.* **74** 1966–83

[16] Park J-M and Lubensky T C 1996 Interactions between membrane inclusions on fluctuating membranes *J. Physique* I **6** 1217–35

[17] Rosso R and Virga E G 1998 Adhesion of lipid tubules in an assembly *Eur. J. Appl. Math.* **9** 485–506
Rosso R and Virga E G 1999 *Eur. J. Appl. Math.* **10** 221 [erratum]

[18] Rosso R and Virga E G 1998 Adhesion by curvature of lipid tubules *Contin. Mech. Thermodyn.* **10** 359–67

[19] Schekman R and Orci L 1996 Coat proteins and vesicle budding *Science* **271** 1526–33

[20] Seifert U and Lipowsky R 1990 Adhesion of vesicles *Phys. Rev.* A **42** 4768–71

[21] Virga E G and Fournier J-B 1995 Equilibrium confocal textures in a smectic-A cell *Rend. Mat. Acad. Lincei* **6** 65–72